Vibronic structure and predissociation dynamics of 2-methoxythiophenol (S$_1$): The effect of intramolecular hydrogen bonding on nonadiabatic dynamics

Jean Sun Lim, Hyun Sik You, So-Yeon Kim, Junggil Kim, Young Choon Park (iD), and Sang Kyu Kim (iD)

View Online   Export Citation   CrossMark

ARTICLES YOU MAY BE INTERESTED IN

Vibronic structure and predissociation dynamics of 2-methoxythiophenol (S₁): The effect of intramolecular hydrogen bonding on nonadiabatic dynamics

View Online   Export Citation   CrossMark

Jean Sun Lim,[a] Hyun Sik You,[b] So-Yeon Kim,[c] Junggil Kim, Young Choon Park,[d] 🔟
and Sang Kyu Kim[e] 🔟

AFFILIATIONS

Department of Chemistry, KAIST, Daejeon 34141, South Korea

[a]**Current address:** Korea Research Institute of Standards and Science (KRISS), Daejeon 34113, South Korea.
[b]**Current address:** LG Chem, LG Science Park, Seoul 07796, South Korea.
[c]**Current address:** LG Chem, R&D Campus, Daejeon 34122, South Korea.
[d]**Current address:** Quantum Theory Project, University of Florida, Gainesville, Florida 32611, USA.
[e]**Author to whom correspondence should be addressed:** sangkyukim@kaist.ac.kr

ABSTRACT

Vibronic spectroscopy and the S–H bond predissociation dynamics of 2-methoxythiophenol (2-MTP) in the S₁ ($\pi\pi^*$) state have been investigated for the first time. Resonant two-photon ionization and slow-electron velocity map imaging (SEVI) spectroscopies have revealed that the S₁–S₀ transition of 2-MTP is accompanied with the planar to the pseudoplanar structural change along the out-of-plane ring distortion and the tilt of the methoxy moiety. The S₁ vibronic bands up to their internal energy of ~1000 cm^{-1} are assigned from the SEVI spectra taken via various S₁ vibronic intermediate states with the aid of *ab initio* calculations. Intriguingly, Fermi resonances have been identified for some vibronic bands. The S–H bond breakage of 2-MTP occurs via tunneling through an adiabatic barrier under the S₁/S₂ conical intersection seam, and it is followed by the bifurcation into either the adiabatic or nonadiabatic channel at the S₀/S₂ conical intersection where the diabatic S₂ state ($\pi\sigma^*$) is unbound with respect to the S–H bond elongation coordinate, giving the excited (Ã) or ground (X̃) state of the 2-methoxythiophenoxy radical, respectively. Surprisingly, the nonadiabatic transition probability at the S₀/S₂ conical intersection, estimated from the velocity map ion images of the nascent D fragment from 2-MTP-d₁ (2-CH₃O–C₆H₄SD) at the S₁ zero-point energy level, is found to be exceptionally high to give the X̃/Ã product branching ratio of 2.03 ± 0.20, which is much higher than the value of ~0.8 estimated for the bare thiophenol at the S₁ origin. It even increases to 2.33 ± 0.17 at the ν_{45}^2 mode (101 cm^{-1}) before it rapidly decays to 0.69 ± 0.05 at the S₁ internal energy of about 2200 cm^{-1}. This suggests that the strong intramolecular hydrogen bonding of S···D···OCH₃ in 2-MTP at least in the low S₁ internal energy region should play a significant role in localizing the reactive flux onto the conical intersection seam. The minimum energy pathway calculations (second-order coupled-cluster resolution of the identity or time-dependent-density functional theory) of the adiabatic S₁ state suggest that the intimate dynamic interplay between the S–H bond cleavage and intramolecular hydrogen bonding could be crucial in the nonadiabatic surface hopping dynamics taking place at the conical intersection.

I. INTRODUCTION

The $\pi\sigma^*$-state mediated photodissociation dynamics of heteroaromatic molecular systems have been both intensively and extensively investigated for the last few decades.[1–3] This subject has attracted much interest as it provides great opportunities to get insights into the ultrafast nonradiative deactivation process of the excited state of biological building blocks as well as nonadiabatic

dynamics at conical intersections in the strong coupling regime of optically active bound and dark unbound states in general. A number of heteroaromatic molecular systems with X–H (X = O, N, S) or X–CH$_3$ moieties attached to the aromatic ring have been targets for such studies, and these include phenols, anisoles, anilines, pyrroles, thiophenols, or thioanisoles.[1–29] As there are already excellent review articles summarizing studies of these systems, we describe only the relevant and necessary information here.

Our group has recently studied the S–H (or D) or S–CH$_3$ (or CH$_{(3−x)}$D$_x$, x = 1–3) bond dissociation dynamics of excited thiophenols[18–24] and thioanisoles,[25–29] respectively. These systems share the prototypical characteristics of the $\pi\sigma^*$-state mediated photodissociation dynamics. Specifically, the first electronically excited state (S$_1$) of the bound $\pi\pi^*$ is crossed by the nearby upper-lying S$_2$ ($\pi\sigma^*$) state which is unbound along the S–Y bond elongation coordinate, giving the first S$_1$/S$_2$ conical intersection. Optically prepared reactive flux bearing the S$_1$ electronic character is then coupled to the S$_2$ state along the diabatic channel correlating with the ground ($\tilde{X}$) state of the C$_6$H$_5$S radical plus the Y fragment. S$_2$ is crossed by the ground (S$_0$) state correlating with the excited ($\tilde{A}$) state of C$_6$H$_5$S fragment, generating the second S$_0$/S$_2$ conical intersection. Here, the C$_6$H$_5$S ($\tilde{X}$) fragment is produced only by the nonadiabatic transition at the second conical intersection, whereas the C$_6$H$_5$S ($\tilde{A}$) channel is the consequence of the adiabatic reaction from the reactive flux sliding on the repulsive S$_2$ state. As the energy difference between the $\tilde{X}$ and $\tilde{A}$ states of the C$_6$H$_5$S radical is only 3000 cm^{-1},[30] it is quite straightforward to estimate the nonadiabatic transition probability from the relative yields of the two channels. Two different translational energy distributions of the Y fragments associated with adiabatic or nonadiabatic channels are clearly manifested as two distinct rings in the velocity-map ion images of Y.

It was found that the S–CH$_3$ bond breakage of thioanisoles takes place mostly on the adiabatic surface, except when the reactive flux is prepared on the conical intersection seam giving dynamic resonances of exceptionally large enhancement of the nonadiabatic transition probability.[25] Recent real-time observation of bifurcating adiabatic and/or nonadiabatic channels of thioanisole at the conical intersection shed new light on the complicated multidimensional nuclear dynamics in the strongly coupled regime of $\pi\pi^*$/$\pi\sigma^*$ electronic surfaces.[27] On the other hand, the overall nonadiabatic transition probabilities in the S–H bond dissociation of thiophenols have been found to be relatively large, giving the $\tilde{X}$/$\tilde{A}$ ratio of ∼0.8 for thiophenol at the S$_1$ zero-point level.[23] The nonadiabatic transition probability of thiophenol slightly depends on the pump wavelength, and yet the structural change induced by the chemical substitution on the phenyl moiety was found to be dramatically influential on the nonadiabatic transition.[16,17,20] Our recent report on 2-fluorothiophenol (2-FTP) and 2-chlorothiophenol (2-CTP) has shown that the intramolecular hydrogen bonding of S···H···F or S···H···Cl, respectively, is responsible for the localization of the reactive flux onto the conical intersection seam in terms of the molecular planarity, resulting in the much higher $\tilde{X}$/$\tilde{A}$ ratio of ∼1.4 or ∼1.1, at the S$_1$ zero-point levels of 2-FTP or 2-CTP, respectively, though the detailed dynamic behavior of the nonadiabatic transition probability with the change of S$_1$/S$_2$ vibronic coupling strength remains as the molecule's own characteristics.[22] In principle, the $\tilde{X}$/$\tilde{A}$ branching ratio is supposed to be proportional to the nonadiabatic transition probability at the second S$_0$/S$_2$ conical intersection.

Nevertheless, S$_1$/S$_2$ and S$_0$/S$_2$ conical intersections encountered along the S–H bond dissociation pathway are connected by the repulsive nσ^* state, and thus, quantum characteristics of the reactive flux beyond the S$_1$/S$_2$ conical intersection are expected to be little modified at the second S$_0$/S$_2$ conical intersection especially with respect to vibrational modes orthogonal to the reaction coordinate. In other words, both S$_1$/S$_2$ and S$_0$/S$_2$ conical intersections share the same branching plane in terms of its gradient and coupling vectors. Furthermore, as those are connected by the repulsive surface where the reactive flux slides very fast along the S–H elongation coordinate, it is most likely that the S$_1$/S$_2$ conical intersection is the fingerprint of the second S$_0$/S$_2$ conical intersection. This rationalizes that the presence of the intramolecular hydrogen bonding facilitates the nonadiabatic passages at both S$_1$/S$_2$ and S$_0$/S$_2$ conical intersections leading to the higher $\tilde{X}$/$\tilde{A}$ branching ratio at the asymptotic limit of 2-FTP or 2-CTP, compared to that of the bare thiophenol.

Herein, we have investigated nonadiabatic dynamics of 2-methoxythiophenol (2-MTP) in order to explore the dynamic effect of the strong intramolecular hydrogen bonding of S···H···OCH$_3$ in 2-MTP on nonadiabatic dynamics in the S–H bond predissociation reaction. The S$_1$ state vibronic structure of 2-MTP has been first revealed here by resonance two-photon ionization (R2PI) and slow-electron velocity map imaging (SEVI) spectroscopic techniques. The excited-state structure and dynamics of 2-MTP are then discussed with the aid of *ab initio* calculations. This work will be a great asset to the understanding of nonadiabatic dynamics in terms of its relationship with the molecular structure.

II. EXPERIMENT

2-MTP-h$_1$ (TCI, >98%) was heated to 95 °C. 2-MTP-d$_1$ (MediGen) was prepared by repeated mixing 2-MTP-h$_1$ with D$_2$O prior to purification. The sample seeded in the Ne carrier gas was expanded into a vacuum chamber through a nozzle orifice (General valve series 9, 0.5 mm diameter) with a baking pressure of 3 atm before being collimated through a 1 mm diameter skimmer. For the R2PI spectra, the molecular beam was crossed by a UV laser pulse in the range of 288.5–267.2 nm (0.4–0.6 mJ/pulse) which was generated by frequency doubling of a dye laser output (Lumonics, HD-500) pumped by a second harmonic output of a Nd:YAG laser (Continuum, Surelite II). The R2PI spectra were obtained by monitoring the parent ion signal which was mass-selected and detected using time-of-flight mass spectrometry. The SEVI and velocity map ion imaging (VMI) experiments were carried out using two independently tunable dye lasers, Scanmate II and Lumonics HD-500. In the (1 + 1′) SEVI experiment,[31,32] the frequency of the pump pulse was fixed at a specific S$_1$ state, while the probe pulse wavelength was varied to obtain photoelectrons just above adiabatic ionization thresholds. In the VMI experiment,[33] the wavelength of the pump laser was fixed at a specific vibronic level of 2-MTP-d$_1$ in the range of 288.5–271.6 nm, whereas the probe beam was used to ionize the nascent D atom fragment using the (2 + 1) ionization at 243 nm and scanned over the entire Doppler width. The ions or photoelectrons were velocity-mapped onto microchannel plates (MCP) coupled to a phosphor screen and recorded with a charge-coupled device (CCD) camera. The polarization direction of the pump pulse was perpendicular to

the time-of-flight axis and the molecular beam, while it was parallel to the plane of the phosphor screen. The polarization direction of the probe beam for the D detection was perpendicular for the sake of the accurate measurement of the anisotropy parameters. The raw photoelectron images obtained in the SEVI experiment were reconstructed using the BASEX algorithm,[34] and the resultant electron kinetic energy distribution was plotted against the internal energy of the cationic ground (D_0) state. The D ion images were reconstructed via the MEVELER program with two hidden layers.[35] The total translational energy distributions were obtained by using the relation $E_T^{tot} = \frac{m_{OCH_3C_6H_4SD}}{m_{OCH_3C_6H_4S}} E_T^D$, where E_T^{tot} is the total translational energy, E_T^D is the kinetic energy of the D fragment, and $m_{OCH_3C_6H_4SD}$ and $m_{OCH_3C_6H_4S}$ are masses of the parent and the radical counterpart of the departing D atom, respectively.

III. COMPUTATIONAL DETAILS

Minimum energy structures of 2-MTP in S_0 and S_1 were optimized using various *ab initio* methods. The S_0 state was calculated by the density functional theory (DFT), second-order Møllet-Plesset perturbation theory (MP2),[36] and second-order coupled-cluster model which employs the resolution of the identity approximation (RICC2).[37,38] The S_1 state structures were obtained by time-dependent density functional theory (TD-DFT) with several functionals, RICC2, configuration interaction singles (CIS),[39] or the complete active space self-consistent field (CASSCF) method.[40,41] The D_0 state was calculated at the B3LYP[42]/6–311++G(3df,3pd) level of theory. The minimum energy path (MEP) on the adiabatic S_1 surface along the S–H elongation coordinate was calculated by relaxing with respect to all nuclear displacement coordinates

except the S–H bond length which was fixed at several points along the reaction pathway using the RICC2/aug-cc-pVDZ method. The MEP was also calculated by B3LYP, CAM-B3LYP,[43] or M06-2X[44] functionals. The rigid scan along the S–H elongation and CCSH dihedral angle coordinates were also carried out using multiconfigurational second order perturbation theory (CASPT2)[45] with a 6–311++G(3df,3pd) basis set, in which the S–H bond length or CCSH angle was varied, whereas all degrees of freedom were fixed at the S_0 minimum geometry. The (10,9) and (12,11) active spaces were employed for the S–H elongation and CCSH dihedral angle coordinates, respectively. An active space with 12 electrons in 11 orbitals (12,11) was comprised of three pairs of π/π^* orbitals, a nonbonding p-orbital of sulfur, σ_{S-H}, σ^*_{S-H}, σ_{C-S}, and σ^*_{C-S} orbitals, whereas the σ_{C-S} and σ^*_{C-S} orbitals were excluded for the (10,9) active space. The RICC2 and CAS calculations were performed using Turbomole v7.0[46] and Molpro 2010.1,[47] respectively, while the rest of methods were conducted using Gaussian 09.[48]

IV. RESULTS AND DISCUSSION

The minimum energy structure of 2-MTP in the ground state is predicted to adopt the planar-cis form where the intramolecular hydrogen bonding of S⋯H⋯OCH$_3$ plays a significant role in directing the planar geometry of the molecule (the supplementary material, Table S1 and Fig. S1). The R2PI spectrum shows the strongest S_1–S_0 origin band at 34 662 cm^{-1}, indicating that the S_1–S_0 optical transition induces little structural change in general, Fig. 1. However, interestingly, a number of low-frequency bands associated with out-of-plane modes are found to be Franck-Condon active, suggesting that the planar to pseudoplanar geometrical change occurs in
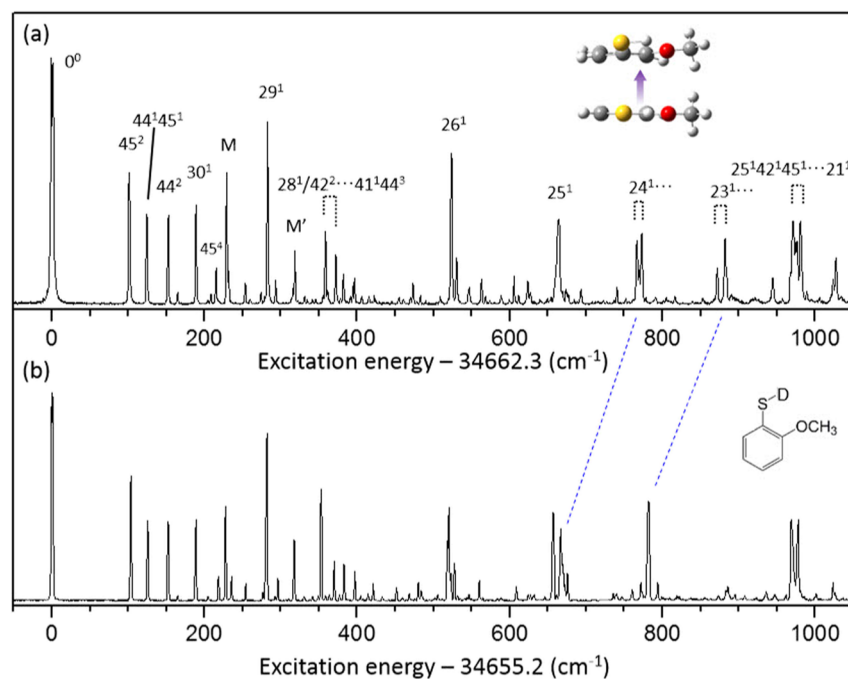

FIG. 1. R2PI spectra of (a) 2-MTP and (b) 2-MTP-d$_1$ up to the S_1 internal energy of 1050 cm^{-1} with vibrational mode assignments for major bands. Spectral features of Fermi resonances are shown as pairs in (a). The molecular structures in the inset are optimized using the RICC2/aug-cc-pVDZ calculation. Blue dashed lines show spectral shifts due to the SH/SD substitution. The mode notation is followed by the Mulliken numbering scheme. M and M′ indicate not-exactly-known modes of mixed characters. See the supplementary material for all detailed mode assignments.

terms of the out-of-plane ring distortion and tilt of the methoxy moiety as manifested by the active excitation of associated ν_{44} and ν_{45} modes in the R2PI spectrum (*vide infra*), giving double minima potentials along such modes as similarly found in the previous spectroscopic study of guaiacol (2-methoxyphenol).[49] The R2PI spectrum of 2-MTP-d_1 (2-CH$_3$O–C$_6$H$_4$SD) seems to be little changed from the undeuterated one except that the spectral origin is ~7 cm^{-1} redshifted, Fig. 1. Most of the low vibrational frequency bands remain unchanged upon the SH/SD substitution, and this is consistent with the fact that those low-frequency modes are associated with out-of-plane ring modes. Large redshifts in the SD isotopomer are found in the 760–900 cm^{-1} region. Specifically, the ν_{24} mode (12 in Varsanyi notation) containing CSH bending at 766/773 cm^{-1} shows a large redshift to 666 cm^{-1}, whereas the 872/882 cm^{-1} band of ν_{23} (CSH bending) also gives the substantial redshift to 782 cm^{-1} by the SH/SD substitution. These spectral shifts are quite consistent with the prediction made by the RICC2/aug-cc-pVDZ calculation. This isotope effect is used for the appropriate vibration assignment (Table S3). As it is nontrivial to assign S_1 vibronic modes, the SEVI technique has been employed in order to get a number of cationic vibrational spectra taken via various S_1 vibronic bands as intermediate states in the $(1 + 1')$ ionization scheme, Fig. 2. According to the propensity rule of $\Delta \nu = 0$, one can deduce the S_1 vibronic characters from the D_0 mode assignments with the aid of *ab initio* calculations (see the supplementary material). Among total 45 normal modes in the C_s symmetry of the D_0 state, modes of 1–30 are in-plane modes (a'), whereas modes of 31–45 are out-of-plane modes (a'') in the Mulliken numbering scheme (See Table S2 for the Varsanyi notation). As expected, the SEVI spectrum taken via the S_1 origin band gives the strongest band at the D_0 origin. The SEVI spectra taken via ν_{45}^2, $\nu_{45}\nu_{44}$, or ν_{44}^2 modes show interesting spectral features. For instance, the SEVI spectrum taken via the 101 cm^{-1} band gives the strongest intensity for the 259 cm^{-1} band in D_0, which is

most likely due to two quanta of ν_{45}^+ corresponding to the out-of-plane torsional motion of the methoxy moiety [inset in Fig. 2(b)]. Similarly, the 152 cm^{-1} S_1 band-mediated SEVI spectrum gives the strongest intensity for the 212 cm^{-1} D_0 band, which is quite likely ascribed to two quanta of ν_{44}^+ associated with the out-of-plane flapping [inset in Fig. 2(d)]. The substantial blueshifts of the ν_{45} and ν_{44} modes in the S_1 to D_0 transition strongly suggest that the S_1 potential energy with respect to these out-of-plane modes is quite shallow, also implying that the S_1 state has double minima potentials along these out-of-plane coordinates. While assignments for most of in-plane modes are quite straightforward according to the propensity rule, the SEVI spectra taken via 229 and 318 cm^{-1} bands show quite complicated spectral features, hampering the one-to-one corresponding mode assignments. These low-frequency modes show the apparent Duschinsky mode mixing. This reflects that the D_0–S_1 transition involves the structural deformation with respect to the multiple out-of-plane ring distortion coordinates. This is in accord with the theoretical prediction that 2-MTP gets the planar structure at the minimum energy of the D_0 state, whereas it adopts the pseudoplanar geometry in the S_1 state having the minimum energy at the nonplanar geometry. This is consistent with the experimental finding that the several out-of-plane modes are strongly observed in the S_1–S_0 R2PI spectrum as well as in the D_0–S_1 SEVI spectrum. It is also interesting to note that prominent doublets or triplets are found in the 760–1000 cm^{-1} region of the S_1–S_0 R2PI spectrum of 2-MTP, and these could possibly be attributed to Fermi resonances (see the supplementary material). As the onset of intramolecular vibrational redistribution (IVR) among S_1 vibrational state manifolds starts from the S_1 energy of 766 cm^{-1} judging from the appearance of the broad background signal in the corresponding SEVI spectra, however, identification and detailed characterization of such doublets lack experimental evidences at the present time and are subject to further investigation.
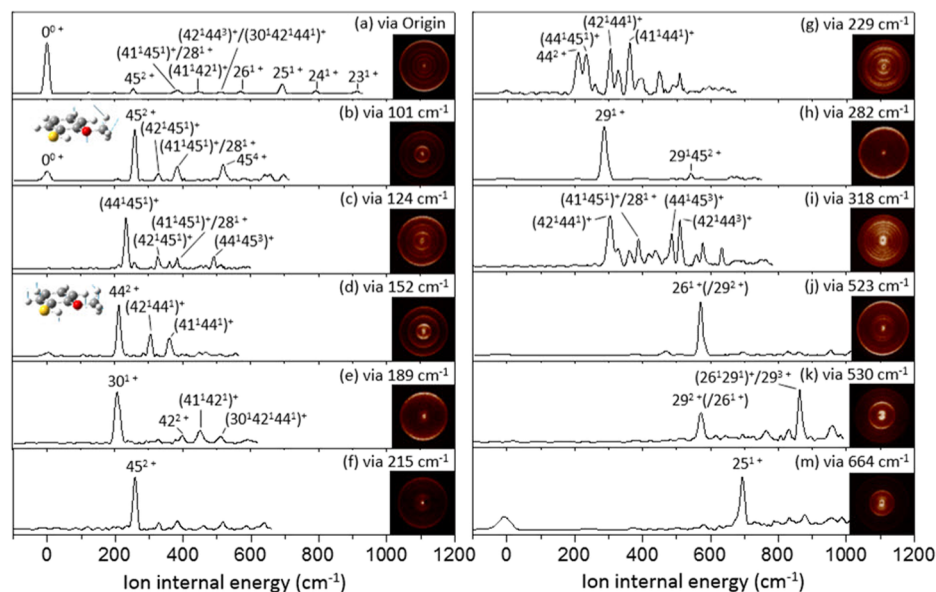

FIG. 2. SEVI spectra of 2-MTP via (a) the S_1 band origin (0^0), (b) 101 cm^{-1} (45^2), (c) 124 cm^{-1} ($44^1 45^1$), (d) 152 cm^{-1} (44^2), (e) 189 cm^{-1} (30^1), (f) 215 cm^{-1} (45^4), (g) 229 cm^{-1} (M; Mixed), (h) 282 cm^{-1} (29^1) (i) 318 cm^{-1} (M') (j) 523 cm^{-1} (26^1), (k) 530 cm^{-1} (29^2; tentative), and (m) 664 cm^{-1} (25^1) bands. The D_0 mode character of ν_{45} (out-of-plane methoxy torsion) and ν_{44} (out-of-plane flapping) calculated by B3LYP/6–311++G(3df,3pd) are displayed in the insets of (b) and (d), respectively. A representative photoelectron image at each intermediate band is shown in the inset.

According to spectroscopic evidences as above, 2-MTP is most likely to adopt the pseudoplanar molecular structure, especially along the ν_{45} and/or ν_{44} vibrational coordinates. These coordinates include the out-of-plane torsion of the OCH$_3$ moiety and the aromatic ring. From the little SH/SD isotope effect on R2PI spectra in the low frequency region, the SH(D) dihedral torsion with respect to the molecular plane does not seem to be activated in the S$_1$–S$_0$ transition because of the strong intramolecular hydrogen bonding of 2-MTP in both ground and excited electronic states. These spectroscopic evidences are consistent with the theoretical prediction by RICC2/aug-cc-pVDZ. Nonplanar minimum energy structure of 2-MPT in S$_1$ is also predicted by TD-DFT and CIS (Fig. S2) but not by CASSCF. The electron density difference map (EDDM) of 2-MTP is quite helpful to understand the origin of molecular nonplanarity (Fig. S6). In the S$_1$ state, the electron density transfers from the nonbonding orbitals of sulfur and oxygen to the aromatic π^* orbital to break the planar aromaticity of the entire molecule. It is also noteworthy that the intramolecular hydrogen bonding of 2-MTP is expected to be weakened in the S$_1$–S$_0$ excitation as the electron density on both the sulfur and oxygen decreases, according to the EDDM. The SH$\cdots$O(CH$_3$) partial bond distance is slightly increased from 2.18 to 2.21 Å upon the S$_1$–S$_0$ excitation according to the RICC2 calculation. The Gaussian double-well one-dimensional potential energy function along the out-of-plane ν_{45} mode with the barrier to planarity of 130 cm^{-1} reproduces the experiment very well in terms of vibrational frequencies for ν_{45}^2 and ν_{45}^4 at 101 and 215 cm^{-1}, respectively, as well as their Frank-Condon integrals, Fig. 3. Here, the one-dimensional potential energy function is adopted in the form of $V(x) = \frac{1}{2}kx^2 + A \exp(-ax^2)$, where x is the nominal nuclear displacement, k is the force constant, whereas the shape of the double-well potential function is determined by the
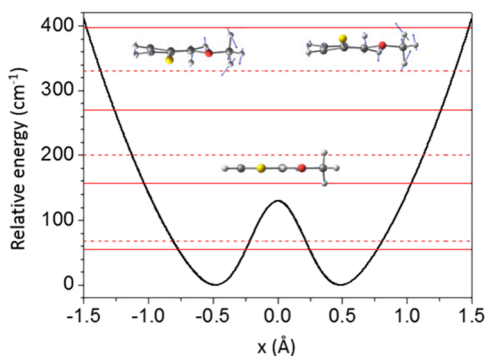
parameters of A and a. It is interesting to note that the similar type of the double-well potential energy function was used in the previous spectroscopic study of guaiacol (2-methoxyphenol) by the Zwier group,[49] giving the barrier to planarity of 195 cm^{-1}.

Total product translational energy distributions obtained from the S–D bond cleavage reaction of 2-MTP-d$_1$ at serval S$_1$ vibronic bands are presented in Fig. 4. It should be noted here that the dissociation dynamics of 2-MTP is expected to be little different from that of 2-MTP-d$_1$ as long as the S–H(D) bond cleavage is concerned. Vibronic dependence of the $\tilde{X}/\tilde{A}$ branching ratio is not expected to be influenced by the SH/SD substitution as most of the S$_1$ low-frequency vibrational modes do not contain the nuclear movement of the SH(D) moiety before IVR prevails at the higher internal energy. Moreover, it was found that the C–H bond cleavage occurs plausibly from unimolecular reaction of vibrationally hot S$_0$ state of thiophenols. This would prohibit the clear-cut interpretation of the
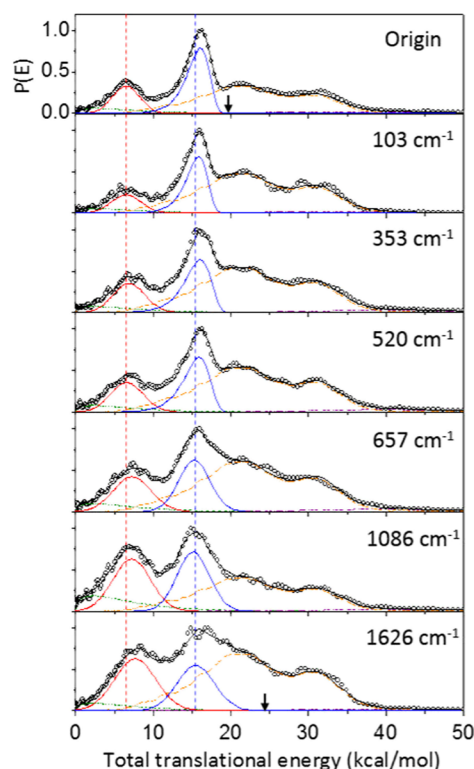

FIG. 3. Gaussian double-well potential along ν_{45} with form of $V = \frac{1}{2}kx^2$ + A exp($-ax^2$). Parameters of A = 203.0 cm^{-1}, a = 9.3 Å^{-2}, and k = 0.0086 mdyne/Å were obtained from the fitting of 45^2 and 45^4 energy levels in the R2PI spectrum. The resultant barrier height is estimated to be 130 cm^{-1} and the relative Franck-Condon factor of 1:0.5:0.1 is calculated for the origin, 45^2, and 45^4 modes, respectively. The red solid and dashed lines represent symmetrically allowed and forbidden transition levels, respectively. The motions in the upper inset are ν_{45} in the S$_1$ state obtained by the calculation at the RICC2/aug-cc-pVDZ level of theory, from which the associated reduced mass is also taken. Eigenvalues and eigenfunctions from this model potential function were obtained using the Wavepacket 4.7.3 program,[50] where the time-independent Schrödinger equation was solved by the Fourier grid Hamiltonian method.

FIG. 4. Total translational energy distributions (black circles) from 2-MTP-d$_1$ at several S$_1$ internal energies. The distributions are decomposed into the $\tilde{X}$ (blue lines) and $\tilde{A}$ (red lines) states of 2-methoxythiophenoxyl radical cofragments, probe-only background (orange dashed lines), and multiphoton statistical component (olive and purple dashed lines). Multiphoton components show the quadratic power dependence on the pump laser intensity, while details for the fits are given in the supplementary material. Black lines, which are the sum of the above five components, are final fits to the experimental distributions. The blue (red) dashed line corresponds to the mean value of the translational energy of the $\tilde{X}$ ($\tilde{A}$) state peak at the excitation energy of band origin. The arrows indicate the maximum available translational energies for the nonadiabatic channel leading to the $\tilde{X}$ state radical.

experiment as we are aiming to focus on the S–H(D) bond dissociation dynamics. Possible unwanted H atom fragments from trace amounts of hydrocarbons in the vacuum chamber could also be avoided by using the 2-MTP-d_1 instead of 2-MTP. The S–D bond predissociation of 2-MTP-d_1, as similarly found in bare thiophenol, 2-FTP, or 2-CTP, occurs via tunneling through the adiabatic barrier under the S_1/S_2 conical intersection seam. This is manifested by the nearly unchanged mean values of the product distributions with the increase of the excitation energy (dashed lines in Fig. 4). Optical excitation to the S_1 bound state is quantum mechanically coupled to S_2, which is repulsive along the S–D bond elongation. The reactive flux on the repulsive S_2 state then bifurcates into adiabatic or nonadiabatic channels at the second S_0/S_2 conical intersection to produce either the excited (Ã) or ground (X̃) state of the $C_6H_4(OCH_3)S\cdot$ radical, respectively. Accordingly, the total translational energy distributions deduced from VMI data of the nascent D fragment show bimodal distributions. The higher kinetic energy component centered at about 16 kcal/mol corresponds to fragments from the nonadiabatic transition (X̃ state), whereas the lower kinetic energy centered at about 7 kcal/mol component is attributed to the adiabatic channel (Ã state). It is notable that the difference between the mean values of the two distinct components in Fig. 4 is estimated to be ~8.86 kcal/mol, which is slightly larger than the X̃–Ã energy gap of the $C_6H_5S\cdot$ radical (8.58 kcal/mol).[30] The components in the high kinetic energy region (orange dashed line) are the background signal of probe-laser only. As thiophenols absorb strongly at 243 nm, the same photon is used to both pump and probe the D fragment. The 243 nm dynamics of thiophenol had been thoroughly investigated in the previous study.[24]

The most intriguing result here is that the S–D predissociation reaction of 2-MTP-d_1 at the S_1 origin gives rise to the very large X̃/Ã product branching ratio of 2.03 ± 0.20, indicating that the nonadiabatic transition probability at the S_0/S_2 conical intersection is exceptionally high, Fig. 5. This branching ratio is much higher than the value of ~0.8 estimated for the bare thiophenol-d_1 at its S_1 zero-point energy level.[23] It is even higher than the X̃/Ã branching ratio of ~1.4 or ~1.1 measured for 2-FTP-d_1 or

2-CTP-d_1 at their S_1 origins, respectively.[22] As these *ortho*-substituted thiophenols adopt the planar geometry aided by the intramolecular hydrogen bonding, their higher X̃/Ã product ratios compared to that of the bare thiophenol-d_1 could be ascribed to the deep localization of the reactive flux onto the planar S_0/S_2 conical intersection, facilitating the nonadiabatic transition to produce the X̃ state of the associated radical. The presumably even stronger intramolecular hydrogen bonding of S–D⋯O(CH$_3$) in 2-MTP-d_1 compared to that of S–D⋯F or S–D⋯Cl in 2-FTP-d_1 or 2-CTP-d_1, respectively, which may retain during the entire reaction pathway, could be responsible for the higher X̃/Ã branching ratio observed for 2-MTP-d_1 although further clarification is desirable in the near future.

The more interesting experimental finding is that the X̃/Ã branching ratio increases to 2.33 ± 0.17 at the S_1 vibronic band of 2-MTP at 101 cm^{-1} (ν_{45}^2), which is even higher compared to that of 2.0 at the S_1 origin, whereas it rapidly decreases thereafter to give 0.69 ± 0.05 at ~2200 cm^{-1}. Apparently, this indicates that the ν_{45}^2 mode excitation specifically facilitates the nonadiabatic transition at the S_0/S_2 conical intersection. Because the initially prepared reactant flux at the S_1 bound state undergoes multidimensional tunneling to the repulsive S_2 state, the rate of tunneling could be strongly mode-dependent unless the energy randomization is not complete, as clearly demonstrated in the recently reported tunneling dynamics studies on the S_1 phenol.[6] This in turn suggests that the tunneling path of the flux at the S_1 origin is somehow different from that prepared at ν_{45}^2, and the latter is more efficient as the nuclear configuration and associated nonadiabatic dynamics at the S_1/S_2 conical intersection seam are likely to be quite similar to those at the S_0/S_2 seam. Specifically, the higher nonadiabatic transition probability at the S_0/S_2 conical intersection could be the consequence from the more efficient S_2–S_1 tunneling through the barrier under the S_1/S_2 conical intersection. Destructive or constructive interference of the nuclear wavefunctions encircled around the conical intersection in the tunneling process, as Guo and colleagues claimed for phenol,[5] might be responsible for this clear mode dependence in the very narrow energy range although quantitative comparison of the experiment with theory seems to be infeasible at the present time. Further theoretical calculations are desirable for the better understanding of the complicated multidimensional events occurring here. The decrease of the X̃/Ã branching ratio with increasing the energy, on the other hand, could be well explained in the polyatomic molecular systems. The reactive flux prepared at the higher S_1 internal energy becomes more dispersed along vibrational degrees of freedom which are orthogonal to the reaction coordinate especially with the progress of IVR, and it tends to stick to the adiabatic path giving rise to the Ã state radical at the asymptotic limit. This may reflect that the conical intersection volume comprising the nonadiabatic funnel is narrowly defined in the vast nuclear configuration space.

In order to obtain better insights into our experimental finding of the exceptionally high nonadiabatic transition probability for 2-MTP, we have carried out the MEP calculation for the adiabatic S_1 state using the relaxed scan along the S–H bond elongation coordinate at the RICC2/aug-cc-pVDZ level of theory. Here, the adiabatic S_1 state is meant to be the lowest singlet excited-state during the whole reaction pathway. As the electronic orbital character transforms from $\pi\pi^*$ to $\pi\sigma^*$, the initial nonplanar S_1 structure in the

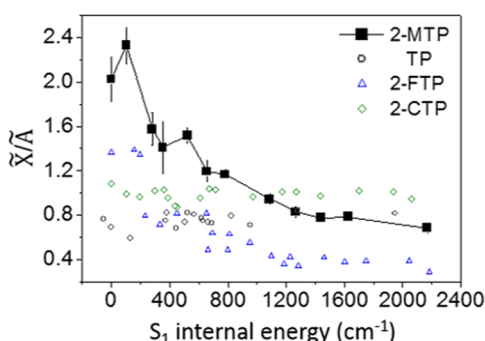
FIG. 5. Plot of the X̃/Ã product ratio vs the S_1 internal energy up to 2400 cm^{-1} for 2-MTP-d_1 (black squares). In addition, those for thiophenol (gray circles), 2-FTP (blue triangles), and 2-CTP (green diamonds) from Refs. 22 and 23 are plotted for comparison. See the supplementary material for the estimation of error bars.
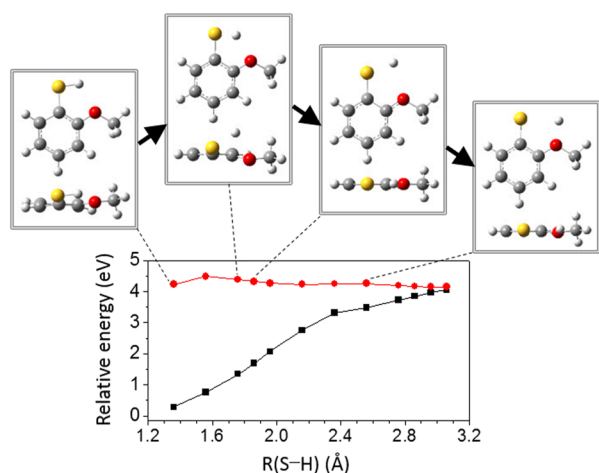
FIG. 6. Energies (red circles) and some geometries along the adiabatic S_1 state calculated at the RICC2/aug-cc-pVDZ level of theory at several fixed S–H bond lengths (see the text for details).

Franck-Condon region becomes planar again along the MEP when the S–H bond length becomes ~1.8 Å. This calculation is in accord with the predicted results made by B3LYP, CAM-B3LYP, or MO6-2X methods using the 6–311++G(d,p) basis set. When the S–H bond length is elongated at about 2.6 Å, the detaching H atom tends to go towards the oxygen atom of the OCH$_3$ moiety, Fig. 6. This intramolecular nuclear rearrangement on the adiabatic S_1 MEP near the S_0/S_2 conical intersection suggests that the dynamic funnel for the nonadiabatic transition is quite narrowly constructed along both S–H elongation and S–H torsional motion, implying that the reactive flux trapped in such an effectively small conical intersection volume would be quite favorable for the nonadiabatic transition. This could be valid as long as it follows the MEP during the entire reaction process, which is quite likely for the reactive flux prepared at the S_1 origin or ν_{45}^2 mode excitation with little internal energy, despite that

our calculation does not guarantee the shape of the potential energy surface in a quantitative way.

The S_1/S_2 surface crossing point of 2-MTP along the one-dimensional S–H elongation coordinate has been calculated to be 4465 cm^{-1} above the S_1 minimum [Fig. 7(a)], providing the upper limit for the adiabatic tunneling barrier in the S_2–S_1 transition. This is much larger than 2085 cm^{-1} calculated for thiophenol at the same level of theory, whereas it is a bit smaller than 5127 cm^{-1} predicted for 2-CTP.[22] Compared to 3936 cm^{-1} calculated for 2-FTP,[22] the S_1/S_2 curve crossing point of 2-MTP is slightly higher. From the experimental fact that the S–H bond dissociation of thiophenol at the S_1 origin takes place within 60 fs,[51] the predissociation of thiophenol should not experience any effective tunneling barrier whatsoever. This indicates that the CASPT2 values of the S_1/S_2 crossing points along the one-dimensional S–H elongation coordinate are significantly overestimated. Yet, the relative order of the curve crossing position among various thiophenols seems to be still quite meaningful as clearly manifested by the experimental finding that the nanosecond S_1–S_0 R2PI spectrum could be nicely obtained for 2-MTP, 2-FTP, or 2-CTP, indicating that the S_1 lifetimes of these *ortho*-substituted thiophenols are much longer than the very brief lifetime of the S_1 thiophenol. The anisotropy parameters of departing fragments from the 2-MTP-d_1 dissociation are estimated to be 0–0.1 (Fig. S7). This indicates that the S–D predissociation should be quite a bit slower than the rotational motion of the whole molecule, washing out the initial geometrical memory of the transition dipole moment aligned with respect to the linear polarization axis of the pump laser pulse. The S_1–S_0 transition dipole moment is predicted to be on the plane and tilted about 63° from the S–D bond axis according to the TD-DFT calculation, suggesting that the small negative value of the anisotropy parameter would be expected were the dissociation prompt.[24]

The last comment could be made on the S–H torsional barrier of the *ortho*-substituted thiophenols. The existence of the intramolecular hydrogen bonding makes it a bit difficult for the S–H bond axis to be placed out of the plane, given the rigidity of the molecular planarity. Our calculation for the SH torsional barrier of 2-MTP gives the value of 2262 cm^{-1} [Fig. 7(b)], which is
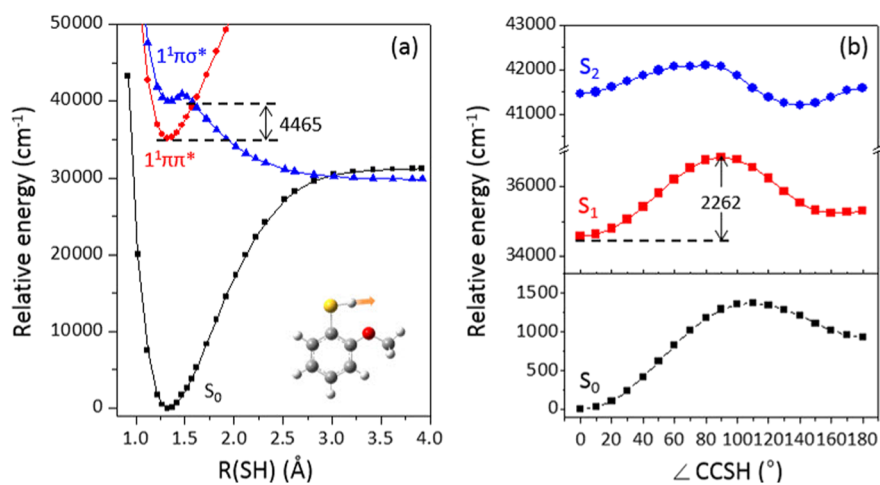

FIG. 7. Potential energy curves for the lowest three singlet states along (a) S–H elongation coordinate in Cs symmetry, and (b) CCSH dihedral angle calculated using CASPT2/SA3-CASSCF/6–311++G(3df,3pd) level of theory with the active space (10,9) and (12,11), respectively.

comparable with the calculated value of 2243 cm^{-1} for 2-FTP, while it is a bit lower than 2665 cm^{-1} calculated for 2-CTP.[22] As the barrier height here is calculated in the Franck-Condon region, its dynamic influence on the nonadiabatic transition during the passage of the flux especially at the S_0/S_2 conical intersection is somewhat vague. Further theoretical consideration would be necessary for full explanation of the experiment in terms of the effect of intramolecular hydrogen bonding on the nonadiabatic transition dynamics in the situation where the coupling vector at the conical intersection branching plane is seemingly parallel with the S–H torsional motion (Fig. S8).

V. CONCLUSIONS

Herein, the S_1 vibronic structure and S–H bond predissociation dynamics of 2-MTP have been thoroughly investigated. The 2-MTP molecule cooled in the molecular jet undergoes the planar to pseudoplanar structural change upon the S_1–S_0 optical transition along the out-of-plane ring distortion and tilt of the methoxy moiety. The S_1 vibronic bands in the Franck-Condon region have been appropriately assigned using the SEVI spectra, revealing that the D_0–S_1 transition is accompanied with the pseudoplanar (S_1) to planar (D_0) structural change and the energy randomization among S_1/S_2 vibronic states starts to occur at 766 cm^{-1} above the S_1 origin. The S–H(D) bond breakage of 2-MTP (2-MTP-d_1) occurs via tunneling through an adiabatic barrier under the S_1/S_2 conical intersection seam, whereas it bifurcates into the adiabatic or nonadiabatic channel at the S_0/S_2 conical intersection. The nonadiabatic transition probability of 2-MTP-d_1 prepared at its S_1 origin is exceptionally high to give the $\tilde{X}/\tilde{A}$ product branching ratio of 2.0± whereas it instantly goes up to 2.3± at the v_{45}^2 mode (101 cm^{-1}) before it finally deceases to 0.7± at ~2000 cm^{-1} above the S_1 origin. The strong intramolecular hydrogen bonding of S···D···OCH$_3$ in 2-MTP-d_1 may be responsible for enforcing the reactive flux to be localized onto the planar conical intersection seam. The minimum energy pathway calculation using the RICC2 method on the adiabatic S_1 state suggests that the intimate dynamic interplay between the S–H bond cleavage and intramolecular hydrogen bonding of the departing H atom to the adjacent OCH$_3$ moiety on the predissociative S_1 state could be crucial in the nonadiabatic surface hopping dynamics taking place in the proximity of the conical intersection. Further high-level theoretical calculations on these interesting systems would be quite desirable as such efforts could resolve an important issue such as the environmental effect on nonadiabatic dynamics especially in the presence of intra- or interhydrogen bonding, which is ubiquitous in nature.

SUPPLEMENTARY MATERIAL

See the supplementary material for the geometries and energetics in the S_0 state and geometries of the S_1 state, full R2PI spectra and UV-UV depletion spectroscopy, vibrational frequencies and assignments of S_0, D_0, and S_1 modes, full assignments of SEVI spectra, electron density difference map (EDDM) for the S_1–S_0 transition, velocity-mapped D ion images, details of the fitting procedure for the deconvolution of total translational energy distributions, and calculated branching space of CI-1.

REFERENCES

[1] A. L. Sobolewski et al., Phys. Chem. Chem. Phys. **4**, 1093 (2002).
[2] M. N. R. Ashfold et al., Science **312**, 1637 (2006).
[3] H. S. You et al., Int. Rev. Phys. Chem. **34**, 429 (2015).
[4] A. L. Sobolewski and W. Domcke, J. Phys. Chem. A **105**, 9275 (2001).
[5] C. Xie et al., J. Am. Chem. Soc. **138**, 7828 (2016).
[6] K. C. Woo and S. K. Kim, J. Phys. Chem. A **123**, 1529 (2019).
[7] D. J. Hadden et al., Phys. Chem. Chem. Phys. **13**, 4494 (2011).
[8] G. M. Roberts et al., J. Am. Chem. Soc. **134**, 12578 (2012).
[9] J. O. F. Thompson et al., J. Chem. Phys. **142**, 114309 (2015).
[10] W. R. Jhang et al., J. Chem. Phys. **151**, 141101 (2019).
[11] N. C. Cole-Filipiak and V. G. Stavros, Phys. Chem. Chem. Phys. **21**, 14394 (2019).
[12] G. Wu et al., J. Chem. Phys. **142**, 074302 (2015).
[13] G. Wu et al., J. Chem. Phys. **144**, 014309 (2016).
[14] K. C. Woo and S. K. Kim, Phys. Chem. Chem. Phys. **21**, 14387 (2019).
[15] T. S. Venkatesan et al., J. Chem. Phys. **136**, 174312 (2012).
[16] T. A. A. Oliver et al., J. Phys. Chem. A **116**, 12444 (2012).
[17] B. Marchetti et al., J. Chem. Phys. **147**, 013923 (2017).
[18] J. S. Lim et al., Angew. Chem., Int. Ed. **45**, 6290 (2006).
[19] I. S. Lim et al., J. Chem. Phys. **126**, 034306 (2007).
[20] J. S. Lim, Y. S. Lee, and S. K. Kim, Angew. Chem., Int. Ed. **47**, 1853 (2008).
[21] J. S. Lim et al., J. Phys. Chem. A **113**, 10410 (2009).
[22] S. Han et al., J. Phys. Chem. A **118**, 6940 (2014).
[23] H. S. You et al., J. Phys. Chem. Lett. **6**, 3202 (2015).
[24] J. S. Lim et al., J. Phys. Chem. A **123**, 2634 (2019).
[25] J. S. Lim and S. K. Kim, Nat. Chem. **2**, 627 (2010).
[26] S. Han et al., J. Chem. Phys. **140**, 054307 (2014).
[27] K. C. Woo, D. H. Kang, and S. K. Kim, J. Am. Chem. Soc. **139**, 17152 (2017).
[28] S.-Y. Kim, J. Lee, and S. K. Kim, Phys. Chem. Chem. Phys. **19**, 18902 (2017).
[29] J. S. Lim et al., Chem. Sci. **10**, 2404 (2019).
[30] J. B. Kim et al., Phys. Chem. Chem. Phys. **13**, 17378 (2011).
[31] C. Nicole et al., Phys. Rev. Lett. **85**, 4024 (2000).
[32] D. M. Neumark, J. Phys. Chem. A **112**, 13287 (2008).
[33] A. T. J. B. Eppink and D. H. Parker, Rev. Sci. Instrum. **68**, 3477 (1997).
[34] V. Dribinski et al., Rev. Sci. Instrum. **73**, 2634 (2002).
[35] B. Dick, Phys. Chem. Chem. Phys. **16**, 570 (2014).
[36] A. E. Azhary et al., J. Chem. Phys. **108**, 5185 (1998).
[37] O. Christiansen, H. Koch, and P. Jørgensen, Chem. Phys. Lett. **243**, 409 (1995).
[38] F. Weigend et al., Chem. Phys. Lett. **294**, 143 (1998).
[39] J. B. Foresman et al., J. Phys. Chem. **96**, 135 (1992).
[40] P. J. Knowles and H.-J. Werner, Chem. Phys. Lett. **115**, 259 (1985).
[41] H. J. Werner and P. J. Knowles, J. Chem. Phys. **82**, 5053 (1985).
[42] A. D. Becke, Phys. Rev. A **38**, 3098 (1988).
[43] T. Yanai, D. P. Tew, and N. C. Handy, Chem. Phys. Lett. **393**, 51 (2004).
[44] Y. Zhao and D. G. Truhlar, J. Phys. Chem. A **110**, 5121 (2006).
[45] P. Celani and H.-J. Werner, J. Chem. Phys. **112**, 5546 (2000).
[46] TURBOMOLE V7.0.2 2015, a development of University of Karlsruhe and Forschungszentrum Karlsruhe GmbH, 1989–2007, TURBOMOLE GmbH, since 2007; available from http://www.turbomole.com.

[47] H.-J. Werner *et al.*, MOLPRO version 2010.1.

[48] M. J. Frisch *et al.*, GAUSSIAN 09, Revision D.1, Gaussian, Inc., Wallingford, CT, 2009.

[49] J. C. Dean *et al.*, J. Chem. Phys. **139**, 144313 (2013).

[50] B. Schmidt and U. Lorentz, WavePacket 4.7: A Program Package for Quantum-Mechanical Wavepacket Propagation and Time-Dependent Spectroscopy available via http://wavepacket.sourceforge.net.

[51] V. Ovejas *et al.*, Chem. Phys. Lett. **661**, 206 (2016).